Electrochemical Deposition of Mesoporous Crystalline Oxide Semiconductor Films from Lyotropic Liquid Crystalline Phases

Hongmei Luo,† Junfeng Zhang,‡ and Yushan Yan*,†

Department of Chemical and Environmental Engineering and Department of Earth Sciences, University of California, Riverside, California 92521

Received June 20, 2003. Revised Manuscript Received July 24, 2003

Direct templating with lyotropic liquid crystalline phases of nonionic surfactants has now been extended to fabricate mesoporous crystalline oxide semiconductors. ZnO and Cu_2O films have been prepared on ITO-covered glass substrates by electrochemical deposition from lyotropic liquid crystalline phases with polyoxyethylene surfactant. The templates and the films are characterized by polarized-light optical microscopy (POM), low-angle and wide-angle X-ray diffraction (XRD), scanning electron microscopy (SEM), transmission electron microscopy (TEM), and UV−vis light absorption spectroscopy.

1. Introduction

Porous crystalline oxide semiconductor films are of considerable interest for numerous technological applications, including dye-sensitized solar cells, chemical sensors, and photocatalysis. Good candidates for these applications are zinc oxide (ZnO) and copper(I) oxide (Cu_2O) because of their optical transparency, nontoxicity, and chemical and photochemical stability.[1−5] ZnO is an *n*-type wide band gap semiconductor, and Cu_2O is a *p*-type semiconductor. ZnO thin films can be produced by magnetron sputtering, chemical vapor deposition, and molecular beam epitaxy. Techniques for making Cu_2O films include thermal oxidation, chemical oxidation, and vacuum evaporation. However, among all of the deposition techniques, electrochemical deposition is particularly attractive because of its low cost and simplicity. Cathodic electrodeposition has been studied for deposition of ZnO and Cu_2O films from aqueous solution.[6−12] Nanoporous ZnO films have been electrodeposited using electrolytes of $Zn(NO_3)_2$ or $ZnCl_2$ in propylene carbonate (PC).[4] Very recently, nanoporous amorphous ZnO films with lamellar structure were electrodeposited utilizing cooperative surface assembly of anionic surfactant sodium dodecyl sulfate (SDS) at very low concentration and inorganic species $Zn(NO_3)_2$ under the influence of an electrostatic potential.[5]

Lyotropic liquid crystalline phases of polyoxyethylene surfactants can be utilized as versatile nanoscale molds for the formation of highly ordered mesoporous materials.[13] Using this approach, mesoporous platinum, tin, palladium, cobalt, nickel, selenium, and tellurium films have been electrodeposited.[13] We have also produced metal, semiconductor, conductive polymer nanowires, and hollow silica fibers by the use of liquid crystalline phases as templates.[14] Here we report the first synthesis of mesoporous crystalline oxide semiconductor films with hexagonal structure via the liquid crystal templating electrodeposition route. The ability to electrodeposit oxide semiconductor films that have well-defined mesoporous nanoarchitectures is important for applications in sensors, solar cells, and photocatalysis.

* To whom correspondence should be addressed. E-mail: yushan.yan@ucr.edu.

† Department of Chemical and Environmental Engineering.

‡ Department of Earth Sciences.

(1) Pal, B.; Sharon, M. *Mater. Chem. Phys.* **2002**, *76*, 82.

(2) Sharma, P.; Mansingh, A.; Sreenivas, K. *Appl. Phys. Lett.* **2002**, *80*, 553.

(3) Chen, S. G.; Kumar, R. V.; Gedanken, A.; Zaban, A. *Israel J. Chem.* **2001**, *41*, 51.

(4) O'Regan, B.; Schwartz, D. T.; Zakeeruddin, S. M.; Grätzel, M. *Adv. Mater.* **2000**, *12*, 1263. O'Regan, B.; Sklover, V.; Grätzel, M. *J. Electrochem. Soc.* **2001**, *148*, C498.

(5) Choi, K.-S.; Lichtenegger, H. C.; Stucky, G. D. *J. Am. Chem. Soc.* **2002**, *124*, 12402.

(6) Izaki, M.; Omi, T. *J. Electrochem. Soc.* **1996**, *143*, L53. Izaki, M.; Omi, T. *J. Electrochem. Soc.* **1997**, *144*, 1949. Izaki, M.; Omi, T. *Appl. Phys. Lett.* **1996**, *68*, 2439. Izaki, M. *J. Electrochem. Soc.* **1999**, *146*, 4517.

(7) Peulon, S.; Lincot, D. *Adv. Mater.* **1996**, *8*, 166. Peulon, S.; Lincot, D. *J. Electrochem. Soc.* **1998**, *145*, 864. Pauporté, Th.; Lincot, D. *Appl. Phys. Lett.* **1999**, *75*, 3817. Pauporté, Th.; Lincot, D. *Electrochim. Acta* **2000**, *45*, 3345. Pauporté, Th.; Cortès, R.; Froment, M.; Beaumont, B.; Lincot, D. *Chem. Mater.* **2002**, *14*, 4702.

(8) Gu, Z. H.; Fahidy, T. Z. *J. Electrochem. Soc.* **1999**, *146*, 156.

(9) Rakhshani, A. E.; Varghese, J. *Thin Solid Films* **1988**, *157*, 87.

(10) Golden, T. D.; Shumsky, M. G.; Zhou, Y.; VanderWerf, R. A.; Van Leeuwen, R, A.; Switzer, J. A. *Chem. Mater.* **1996**, *8*, 2499. Bohannan, E. W.; Shumsky, M. G.; Switzer, J. A. *Chem. Mater.* **1999**, *11*, 2289;. Barton, J. K.; Vertegel, A. A.; Bohannan, E. W.; Switzer, J. A. *Chem. Mater.* **2001**, *13*, 952.

(11) de Jongh, P. E.; Vanmaekelbergh, D.; Kelly, J. J. *Chem. Mater.* **1999**, *11*, 3512.

(12) Georgieva, V.; Ristov, M. *Sol. Energy Mater. Sol. Cells* **2002**, *73*, 67.

(13) Attard, G. S.; Bartlett, P. N.; Coleman, N. R. B.; Elliott, J. M.; Owen, J. R.; Wang, J. H. *Science* **1997**, *278*, 838. Elliott, J. M.; Attard, G. S.; Bartlett, P. N.; Coleman, N. R. B.; Merckel, D. A. S.; Owen, J. R. *Chem. Mater.* **1999**, *11*, 3602. Attard, G. S.; Elliott, J. M.; Bartlett, P. N.; Whitehead, A.; Owen, J. R. *Macromol. Symp.* **2000**, *156*, 179. Bartlett, P. N.; Gollas, B.; Guerin, S.; Marwan, J. *Phys. Chem. Chem. Phys.* **2002**, *4*, 3835. Bartlett, P. N.; Birkin, P. N.; Ghanem, M. A.; de Groot, P.; Sawicki, M. *J. Electrochem. Soc.* **2001**, *148*, C119. Nelson, P. A.; Elliott, J. M.; Attard, G. S.; Owen, J. R. *Chem. Mater.* **2002**, *14*, 524. Nandhakumar, I.; Elliott, J. M.; Attard, G. S. *Chem. Mater.* **2001**, *13*, 3840. Gabriel, T.; Nandhakumar, I. S.; Attard, G. S. *Electrochem. Commun.* **2002**, *4*, 610.

(14) Huang, L. M.; Wang, H. T.; Wang, Z. B.; Mitra, A.; Bozhilov, K. N.; Yan, Y. S. *Adv. Mater.* **2002**, *14*, 61. Huang, L. M.; Wang, H. T.; Wang, Z. B.; Mitra, A.; Zhao, D. Y.; Yan, Y. S. *Chem. Mater.* **2002**, *14*, 876. Huang, L. M.; Wang, H. T.; Hayashi, C. Y.; Tian, B. Z.; Zhao, D. Y.; Yan, Y. S. *J. Mater. Chem.* **2003**, *13*, 666.

10.1021/cm0345218 CCC: $25.00
Published on Web 08/28/2003

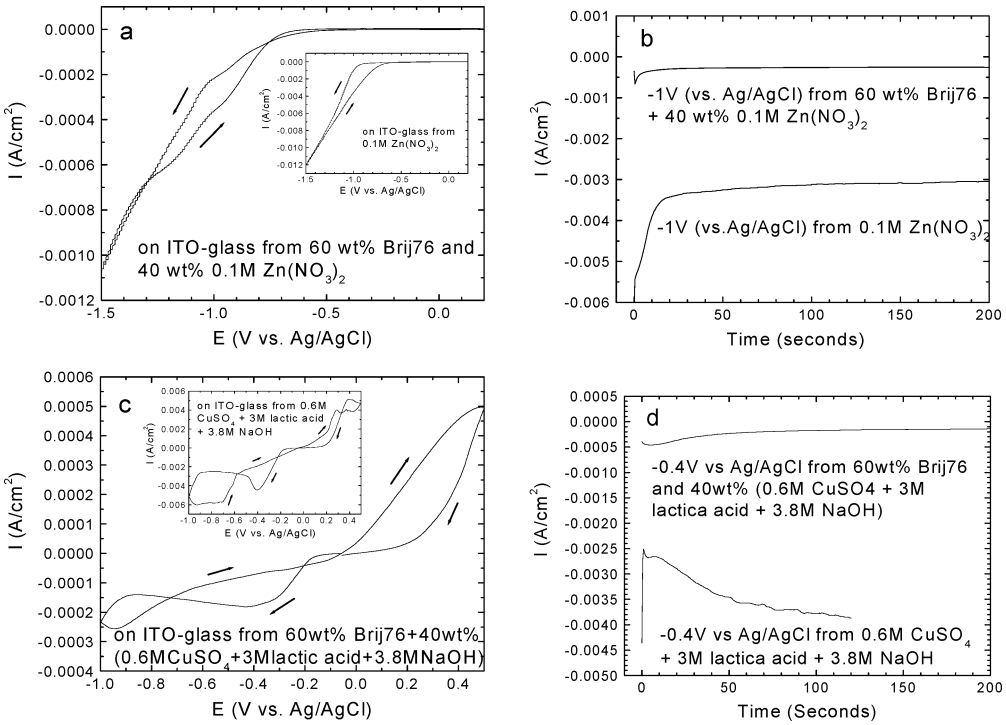

Figure 1. (a) Cyclic voltammogram (CV) of film deposition on ITO-glass from mesoporous ZnO electrolyte, inset for CV from ZnO electrolyte; (b) variation of the cathode current with time from ZnO and mesoporous ZnO electrolyte for deposition at −1 V vs Ag/AgCl; (c) CV of film deposition from mesoporous Cu_2O electrolyte, inset for CV from Cu_2O electrolyte; (d) variation of the cathode current with time from Cu_2O and mesoporous Cu_2O electrolyte for deposition at −0.4 V vs Ag/AgCl.

2. Experimental Section

2.1. Materials. Nonionic surfactants polyoxyethylene(10) cetyl ether (Brij56, $C_{16}EO_{10}$), polyoxyethylene(10) stearyl ether (Brij76, $C_{18}EO_{10}$), and polyoxyethylene(20) stearyl ether (Brij78, $C_{18}EO_{20}$) were purchased from Aldrich. Zinc nitrate ($Zn(NO_3)_2 \cdot 6H_2O$, 99.998%), copper sulfate ($CuSO_4 \cdot 5H_2O$, 98−102%), lactic acid (ACS, 85−90%), sodium hydroxide (NaOH, 99%), acetone (ACS, 99.5+ %), and platinum gauze (Pt, 99.9%) were obtained from Alfa Aesar. Ag/AgCl (3M NaCl) electrode was from Bioanalytical systems, Inc. Indium tin oxide (ITO)-coated glass plates (ITO thickness 175±25 nm, resistance 6±2 Ω) were from Delta Technologies. Distilled water was passed through a Barnstead system until its resistivity reached 17 MΩ·cm. Prior to electrodeposition, the glass was rinsed ultrasonically in acetone for 10 min, and then rinsed in distilled water for another 10 min. All the other chemicals were used as received.

2.2. Preparation of Liquid Crystalline Phase. The electrolyte used in the electrodeposition of mesoporous ZnO films was a binary system of a 60 wt % Brij76 surfactant and a 40 wt % 0.1 M $Zn(NO_3)_2$ (pH of the aqueous solution was 6). For mesoporous Cu_2O films deposition, the electrolyte consisted of a 60 wt % Brij76 surfactant and a 40 wt % aqueous solution with composition of 0.6 M $CuSO_4$, 3 M lactic acid, and 3.8 M NaOH (pH of the solution was adjusted to around 9 by the addition of several drops of 5 M NaOH). To prepare the liquid crystal, the surfactant was first heated to around 50−60 °C to be melted, and then the aqueous solution was added dropwise with stirring. A clear viscous liquid was obtained after 10 min.

2.3. Electrodeposition. The experiment was performed in a standard three-electrode glass cell, which was immersed in a water bath held at 65 °C. ITO-glass was used as the cathode with Pt gauze as the anode and Ag/AgCl electrode as the reference electrode. Electrodeposition was carried out using a Solartron 1287 potentiostat. After deposition, the film was rinsed in purified water to remove the surfactant mixture. Unless otherwise specified, nonporous ZnO film was electrodeposited on ITO-glass at −1 V vs Ag/AgCl from 0.1 M $Zn(NO_3)_2$, and mesoporous ZnO film was from 60 wt % Brij 76 and 40 wt % 0.1 M $Zn(NO_3)_2$. Nonporous Cu_2O film was deposited at −0.4 V vs Ag/AgCl from 0.6 M $CuSO_4$ + 3 M lactic acid + 3.8 M NaOH, and mesoporous Cu_2O film was from 60 wt % Brij 76 and 40 wt % (0.6 M $CuSO_4$ + 3 M lactic acid + 3.8 M NaOH). The corresponding electrolytes are referred to as ZnO, mesoporous ZnO, Cu_2O, and mesoporous Cu_2O electrolytes, respectively.

2.4. Characterization. Before electrodeposition, the phase behavior of the electrolyte mixture was investigated using a Nikon Microphot-FXA microscope at room temperature. Thin films of the liquid crystals were prepared by sandwiching the mixture between a glass microscope slide and cover slip, and cooling them from 50−60 °C to room temperature. X-ray diffraction (XRD) patterns were recorded on a Siemens D-500 diffractometer using Cu Kα radiation. Scanning electron microscopy (SEM) images were obtained in a Philips XL30-FEG operated at 20 kV. The semiconductor films were coated with Au and Pd before imaging in the SEM. Transmission electron microscopy (TEM) images and electron diffraction (ED) patterns were obtained on a Philips CM300 equipped with energy-dispersive X-ray (EDX) spectrometer and operated at 300 kV. The samples for TEM were prepared by scraping films from the ITO-glass directly onto a carbon-coated copper grid. UV−vis absorbance spectra for the transparent films were taken on a Varian Cary 50 UV−visible spectrophotometer using the ITO-glass as reference.

3. Results and Discussion

3.1. Electrochemical Studies. The cyclic voltamogram of film deposition from mesoporous ZnO electrolyte (Figure 1a) at a scan rate of 10 mV/s over the potential range +0.2 to −1.5 V is similar to that of deposition from nonporous ZnO electrolyte (inset in Figure 1a). The sweep starts at open-circuit potential about + 0.2 V. There is essentially no current when the cathode potential is greater than −0.6 V. Below −0.7 V, the cathode current increases gradually with potential, indicating that ZnO starts to grow. The mechanism of

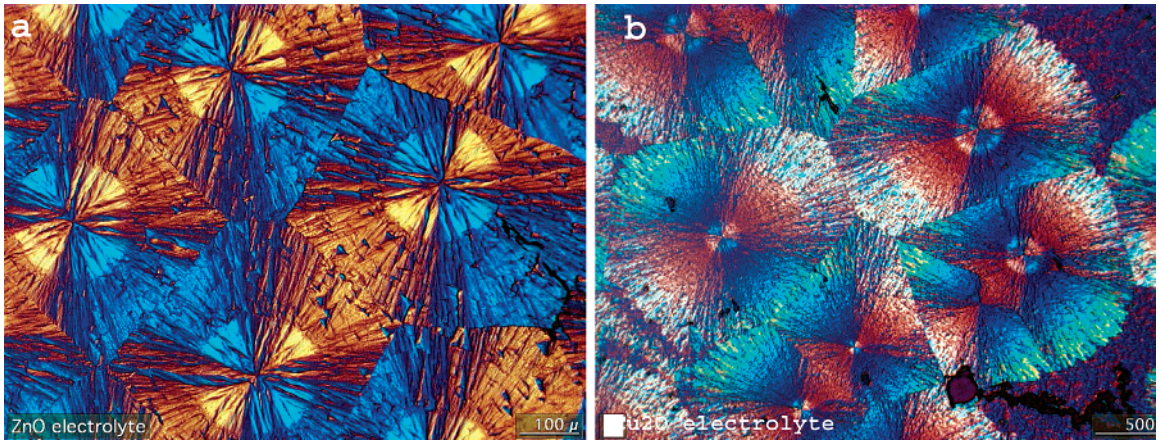

Figure 2. Polarized-light optical microscopy (POM) images using gypsum plate filters for mesoporous ZnO electrolyte (a) and mesoporous Cu_2O electrolyte (b).

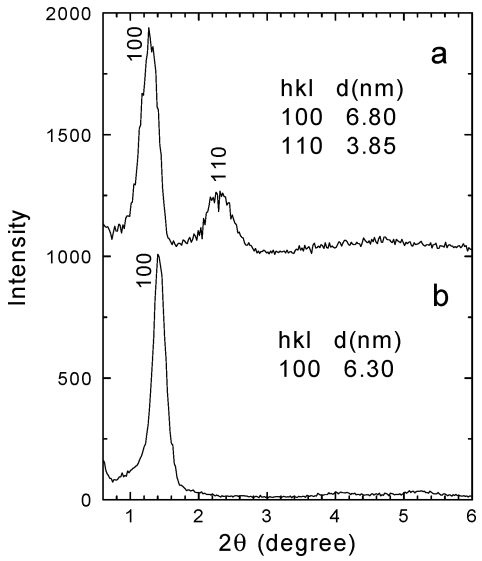

Figure 3. Low-angle XRD patterns for mesoporous ZnO electrolyte (a) and mesoporous Cu_2O electrolyte (b).

deposition of ZnO film from $Zn(NO_3)_2$ aqueous solution has been suggested that nitrate ions were first reduced with an increase of OH^- concentration ($NO_3^- + H_2O + 2e^- \rightarrow NO_2^- + 2OH^-$), and then $Zn(OH)_2$ was formed and converted to ZnO when the deposition was carried out at a slightly elevated temperature of about 65 °C ($Zn^{2+} + 2OH^- \rightarrow Zn(OH)_2 \rightarrow ZnO + H_2O$).[6] Typical time-dependent current behavior under constant cathode potential at −1 V vs Ag/AgCl for nonporous and mesoporous ZnO films is shown in Figure 1b. The currents change quickly during the first 30 s, and then become constant at 0.00027 A/cm^2 for mesoporous ZnO, and 0.0031 A/cm^2 for nonporous ZnO film. It is noted that the current−voltage and current−time curves from electrolytes containing Brij56 or Brij78 surfactants are the same as those for Brij76.

Cyclic voltammetry was also used to study Cu_2O deposition. Cu_2O was electrodeposited by reduction of Cu^{2+} from a Cu(II) lactate aqueous solution with basic pH.[10,11] The linear sweep voltammogram for mesoporous Cu_2O electrolyte is shown in Figure 1c, and compared with that of the nonporous Cu_2O electrolyte (inset in Figure 1c). The deposition of Cu_2O is in a potential window between −0.3 to −0.5 V. If the potential becomes too negative, e.g., below −0.6 V, Cu is co-deposited.[10,11] On the reverse scan, stripping peaks for Cu and Cu_2O oxidation to Cu^{2+} are observed. Time-dependent current behaviors under constant cathode potential at −0.4 V vs Ag/AgCl for nonporous and mesoporous Cu_2O films are shown in Figure 1d. Similar to ZnO, the deposition of mesoporous Cu_2O film has current densities quite lower than those of the nonporous film.

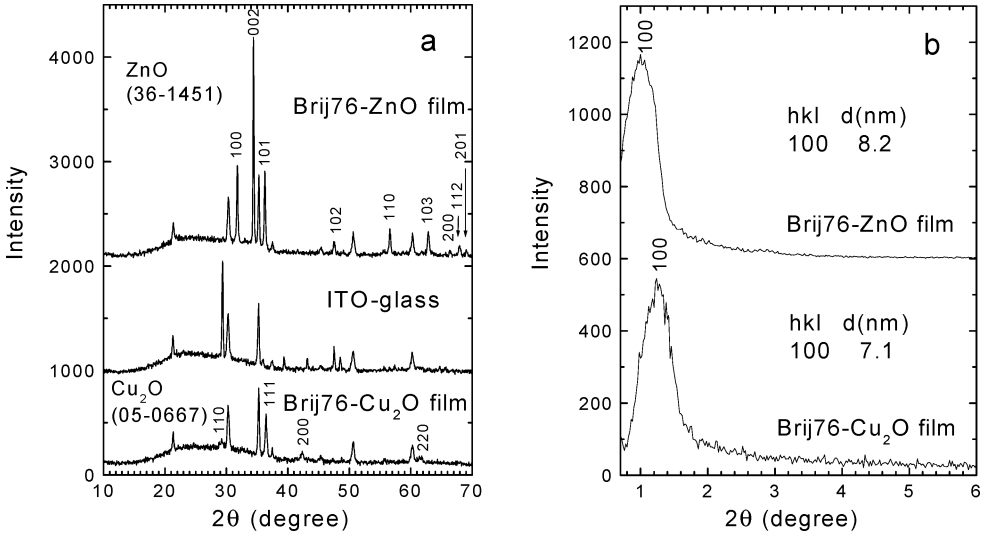

Figure 4. (a) Wide-angle XRD; and (b) low-angle XRD patterns for mesoporous ZnO and Cu_2O films grown on ITO-glass.

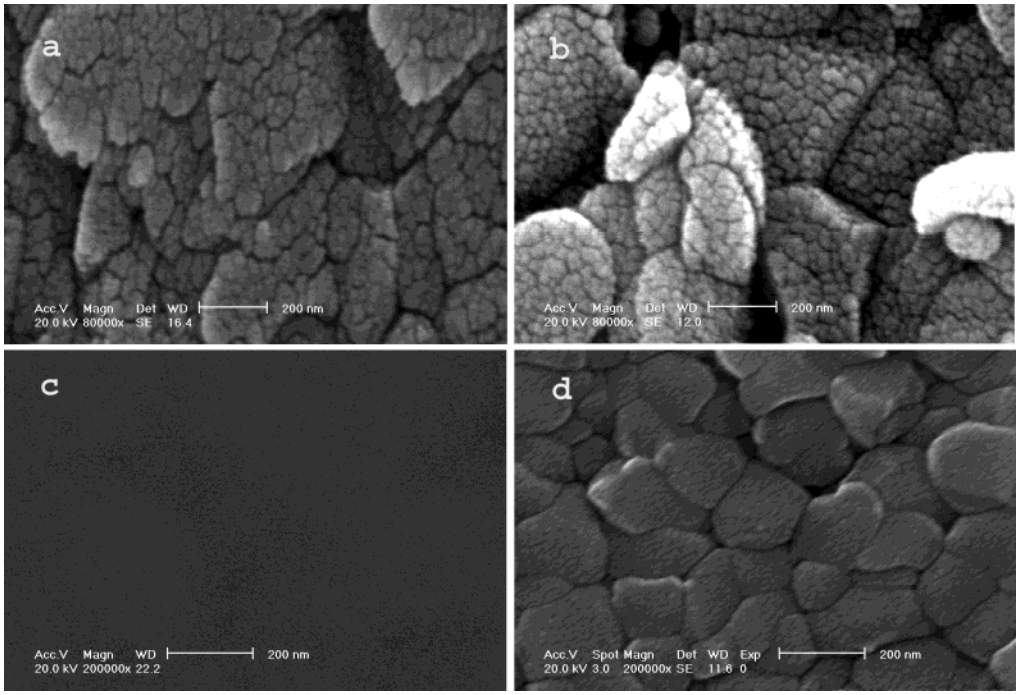

Figure 5. SEM images of ZnO and Cu_2O films on ITO-glass: (a) ZnO film; (b) mesoporous ZnO film; (c) Cu_2O film; (d) mesoporous Cu_2O film.

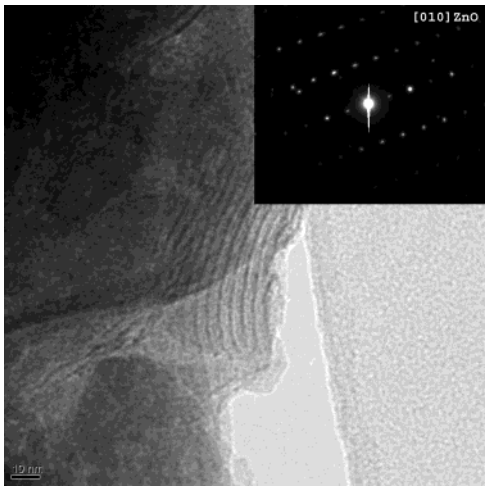

Figure 6. TEM images of mesoporous ZnO film, from side view of pores.

3.2. Phase Characterization. It is demonstrated that electrodeposition of metal (e.g., Pt, Pd, Sn, Ni, Co) or elemental semiconductor (e.g., Se, Te) from lyotropic liquid crystalline phases of nonionic surfactants produces films with well-defined periodic mesoporous nanostructures.[13] Considering the nanostructured film is a direct cast of the structure of the lyotropic phases used to template the deposition, it is important to investigate the phase structure before electrodeposition. Figure 2 shows polarized-light optical microscopy (POM) images for mesoporous ZnO and Cu_2O electrolytes. The equal 120° spacing between the three axes in the same plane is a clear indication of the hexagonal structure.[15,16] The size of the crystal varied with the cooling rate of the thin films of the liquid crystals from 50−60 °C to room temperature.

The electrolyte mixture phase structure was also examined by low-angle XRD (Figure 3). The mesoporous ZnO electrolyte shows two well-resolved peaks with *d* spacing of 6.80 and 3.85 nm (ratio is $1:1/\sqrt{3}$), which can be indexed as (100) and (110) reflections associated with the hexagonal symmetry. From the (100) peak with a *d* spacing of 6.80 nm, the lattice parameter a_0 of 7.85 nm is obtained. The mesoporous Cu_2O electrolyte shows a (100) peak with a *d* spacing of 6.3 nm (a_0 of 7.28 nm).

3.3. XRD, SEM, and TEM. The wide-angle XRD patterns of mesoporous ZnO and Cu_2O films are shown in Figure 4a. Except the substrate peaks, all other peaks belong to hexagonal ZnO (JCPDS no. 36-1451) and cubic Cu_2O (05-0667) without any impurity. It is clear that mesoporous ZnO film shows (0001) preferred orientation, similar to that of nonporous ZnO film.[6]

Low-angle XRD patterns for mesoporous ZnO and Cu_2O films are shown in Figure 4b. The d_{100} values for mesoporous ZnO and Cu_2O films are 8.2 and 7.1 nm, respectively. This corresponds to pore-to-pore distances of 9.4 and 8.2 nm. Low-angle diffraction peaks were not observed for nonporous films deposited in the absence of surfactants. The appearance of low-angle peaks indicates that mesoscopic order in the liquid crystalline templates is preserved in the porous ZnO and Cu_2O films. It is known that the size of pores can be varied by using surfactants of different alkyl chain lengths in the lyotropic liquid crystalline phases.[13] For mesoporous ZnO film, Brij56 or Brij78 was also used as template to form the liquid crystalline phase. As expected, the use of larger surfactant molecule Brij78 caused an increase in the *d* spacing of the resulting mesostructure, whereas Brij56 led to slightly smaller *d* spacing. The d_{100} spacing value for ZnO and Cu_2O films is consistent with the those of mesoporous Pt, Ni, Co films templated from Brij56 and Brij76.[13]

(15) McCrone, W. C.; McCrone, L. B.; Delly, J. G. *Polarized Light Microscopy*; Ann Arbor Science Publishers: Ann Arbor, MI, 1978.
(16) Raimondi, M. E.; Seddon, J. M. *Liq. Cryst.* **1999**, *26*, 305.

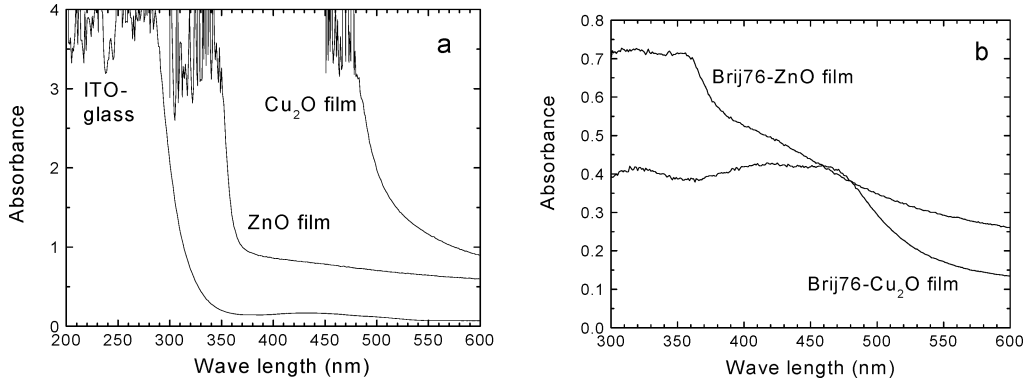

Figure 7. Optical absorbance spectra for (a) ITO-glass, ZnO and Cu_2O films; (b) mesoporous ZnO and Cu_2O film.

The surface morphology of nonporous and mesoporous ZnO and Cu_2O films has been investigated by SEM and is shown in Figure 5. Mesoporous ZnO film has morphology similar to that of nonporous film. The (0001) oriented film is the aggregate of hexagonal columns, and some gaps are seen between the columns. A smooth surface is seen for nonporous Cu_2O film, and mesoporous Cu_2O film shows polycrystalline grains.

Figure 6 shows the TEM image for mesoporous ZnO film. The image reveals a highly ordered mesoporous structure. Light regions in the TEM image correspond to the pores left after surfactant removal, whereas dark regions correspond to the deposited ZnO. The selected area electron diffraction (SAED) (inset in Figure 6) confirms the pure crystalline ZnO formation. The observed parallel lines have a repeat distance of 3 nm, which reveals the hexagonally close-packed cylindrical pores with a uniform pore diameter of 3 nm. The TEM micrograph of mesoporous ZnO is consistent with previous observations of hexagonally oriented channels of other materials, and the pore diameter is also comparable with that found from TEM for mesoporous Pt, Ni, Co, Se, and Te films electrodeposited from the liquid crystalline phase of the same surfactant Brij76 or Brij56.[13] From our work and ref 13, use of the larger-molecule surfactant Brij78 caused an increase in the *d* spacing of the mesostructure from low-angle XRD, and an increase of the pore size from TEM, whereas smaller-molecule Brij56 or Brij76 led to smaller *d* spacing and smaller pore size, and the thickness of the mesoporous wall did not change.

3.4. Optical Properties. ITO-glass substrate is optically transparent from the visible wavelength to 310 nm (4.0 eV) in the ultraviolet region. The band gap of ITO is greater than that reported for bulk ZnO (3.3 eV) and Cu_2O (2.1 eV). This allowed us to measure the band gap of ZnO and Cu_2O films on ITO-glass. Figure 7a shows the optical absorbance spectra for ITO-glass, nonporous ZnO, and Cu_2O films with ITO-glass as reference. The optical absorbance measurement for ZnO film shows it absorbs strongly at wavelengths below 380 nm. ZnO is a direct band gap semiconductor. The plot of $(\alpha h\nu)^2$ versus energy of the photons $h\nu$ is linear, and the energy intercept of the plot gives the direct band gap value, E_g, of 3.3 eV for the electrodeposited ZnO film. Cu_2O is also a direct band-gap semiconductor and an E_g of 2.3 eV is obtained. This is larger than 2.1 eV reported for Cu_2O, but similar to 2.38 eV reported for electrodeposited Cu_2O film in ref 12. The mesoporous ZnO and Cu_2O films have poor optical properties as shown in Figure 7b. It is noted however, that the optical transparency of ZnO films has a strong dependence on surface irregularity and on the existence of defects such as pores.[6]

Acknowledgment. We thank Dr. K. N. Bozhilov for TEM images, and Dr. Limin Huang for valuable discussion of low-angle XRD analysis. We acknowledge the financial support from Riverside Public Utilities, California Energy Commission, and Pacific Fuel Cell Corporation.

CM0345218